

Article

Modulation of Properties by Ion Changing Based on Luminescent Ionic Salts Consisting of Spirobi(boron ketoiminate)

Kazumasa Suenaga, Shunichiro Ito , Kazuo Tanaka *  and Yoshiki Chujo

Department of Polymer Chemistry, Graduate School of Engineering, Kyoto University, Katsura, Nishikyo-ku, Kyoto 615-8510, Japan; artificial.tai@gmail.com (K.S.); ito@poly.synchem.kyoto-u.ac.jp (S.I.); chujo@poly.synchem.kyoto-u.ac.jp (Y.C.)

* Correspondence: tanaka@poly.synchem.kyoto-u.ac.jp; Tel.: +81-75-383-2604; Fax: +81-75-383-2605

Abstract: We report development of luminescent ionic salts consisting of the boron ketoiminate structure, which is one of the robust skeletons for expressing aggregation-induced emission (AIE) properties. From the formation of the boron-centered spiro structure with the ketoiminate ligands, we obtained stable ionic salts with variable anions. Since the ionic salts show T_m s below 100 °C, it was shown that these salts can be classified as an ionic liquid. By using PF₆ anion, the single crystal—which is applicable for X-ray crystallography—was obtained. According to the optical measurements, it was proposed that electronic interaction should occur through the boron center. Moreover, intense emission was observed both in solution and solid. Finally, we demonstrated that the emission color of the PF₆ salt was altered from crystal to amorphous by adding mechanical forces. Based on boron complexation and intrinsic solid-state luminescent characters, we achieved obtainment of emissive ionic materials with environmental responsivity.

Keywords: boron; spiro; ionic salt; luminescence



Citation: Suenaga, K.; Ito, S.; Tanaka, K.; Chujo, Y. Modulation of Properties by Ion Changing Based on Luminescent Ionic Salts Consisting of Spirobi(boron ketoiminate). *Molecules* **2022**, *27*, 3438. <https://doi.org/10.3390/molecules27113438>

Academic Editor: Pradip K. Bhowmik

Received: 7 May 2022

Accepted: 25 May 2022

Published: 26 May 2022

Publisher's Note: MDPI stays neutral with regard to jurisdictional claims in published maps and institutional affiliations.



Copyright: © 2022 by the authors. Licensee MDPI, Basel, Switzerland. This article is an open access article distributed under the terms and conditions of the Creative Commons Attribution (CC BY) license (<https://creativecommons.org/licenses/by/4.0/>).

1. Introduction

Most organic luminescent dyes show poor emission properties in solids due to aggregation-caused quenching (ACQ) induced mainly by non-specific intermolecular interactions. Therefore, for designing film-type sensors and devices based on organic materials, it is essential to load some mechanisms for suppressing ACQ. One of the promising strategies is to apply the class of molecules possessing AIE properties. AIE-active molecules can show intense emission only when they are aggregates. In the solution state, excited states are readily decayed by intramolecular interaction, while emission can be recovered in solid by suppressing molecular motions and intermolecular interactions. As a result, AIE behaviors can be realized. Furthermore, on the basis of potential environmental sensitivity of AIE-active molecules, various types of stimuli-responsive luminochromic materials and sensors have been developed by employing AIE-presenting skeletons [1–3]. For instance, by utilizing aggregation behaviors for signal amplification, a trace amount of water can be detected [4,5]. From this viewpoint, heteroatom-containing molecules with AIE properties are attractive candidates because potential environmental sensitivity of heteroatoms is available for expressing stimuli responsiveness [6–9]. We have also discovered AIE-active boron complexes and developed stimuli-responsive materials by using these molecules as an element-block [10–13], which is a building block containing heteroatoms for constructing functional materials [14–17]. For example, simply by connecting AIE-active boron complexes, AIE-active and solid-state luminescent polymers can be fabricated from heteroatom-containing molecules including boron complexes [18–22]. In particular, since stimuli responsiveness, such as luminochromism as well as intensity changes, was often observed, the series of luminescent sensors can be obtained [23–29]. By replacing boron with a

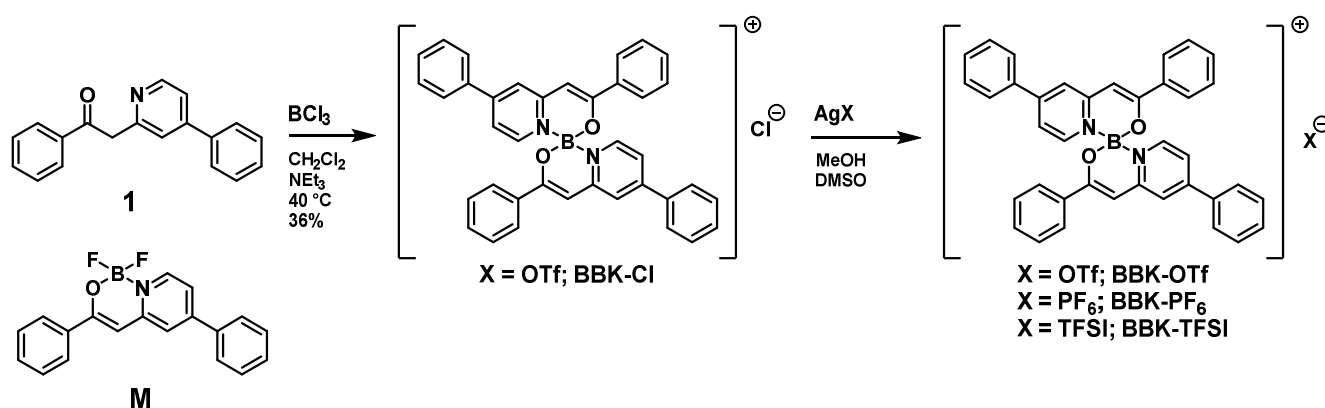
different element, such as other group-13 elements, stimuli responsiveness and/or unique luminescent properties were observed [30–33]. From the changes in emission intensity and color, the target molecules or alteration of environmental factors can be monitored.

In conventional boron complexes, difluoride is very common because of its high stability and low synthetic difficulty. Meanwhile, some research groups tried replacing the two fluoride atoms with another unit [34–42]. The resulting spiro complexes have various unique features originating from cationic character and steric structures. For instance, boron complexes with two diketone ligands were synthesized [34,35]. These compounds showed interesting stimuli responsiveness, such as solvatochromism and thermochromism. Another paper reported that the central boron atom in the bis(1,9-oxido-phenalenyl)boron complex has an intriguing property [40–42]. In these research papers, boron complexes have the spiro structure, where each ligand perpendicularly bridges through the central boron atom. These non-planar spiro structure play key roles in organic electronic devices, such as OLEDs [43], organic phototransistors (OPTs) [44], and organic solid-state lasers (OSSLs) [45]. Spiro structures show chemical and thermal stability and good solubility because of their steric architectures. Further, their bulky structures play a role in lowering melting temperatures (T_m s) and crystallinity. Therefore, spirobifluorene derivatives were used for OLEDs as amorphous emissive materials [45]. Therefore, we designed the new boron complexes consisting of the spiro structure to obtain solid-state luminescent properties and expected stimuli responsiveness in condensed states.

Herein, we report ionic salts consisting of the spiro structure with luminescent properties in solution and solid states. On the basis of the spiro structure with luminescent boron complexes, four types of ionic salts with variable counter anions were prepared. From the thermal analyses, it was observed that all salts have melting temperatures below 100 °C, indicating that the products can be classified as an ionic liquid according to the conventional definition. The ionic salts exhibit intense emission in solid as well as solution. In particular, the PF₆ salt can form single crystal and show different luminescent colors between crystal and amorphous states. Finally, mechanochromic luminescence was observed from the PF₆ salt. We can demonstrate the design of luminescent ionic materials based on boron coordination properties.

2. Results and Discussion

Synthesis of the spirobi(boron ketoiminate) (BBK) structure and salt exchanges were performed according to Scheme 1 according to the previous study [20]. Boron trichloride was added to mixture solution of the ketoimine ligand **1** in the presence of triethylamine in CH₂Cl₂ and stirred at r.t. for 24 h. The salt BBK-Cl was obtained as a yellow solid after freeze-drying. We also prepared BKI as a model compound **M** [20]. From the characterization with ¹H, ¹³C and ¹¹B NMR spectroscopy and a mass measurement, we obtained the expected data. Further, by using BBK-Cl as a platform, we prepared the series of salt compounds with variable anion species. The DMSO solution of BBK-Cl was added to AgOTf in MeCN and stirred at r.t. for 3 h. After removal of the precipitated AgCl using filtration, the yellow solid was obtained through extraction followed by freeze-drying. With this protocol, three kinds of salts were obtained with trifluorosulfonate (OTf⁻), hexafluorophosphate (PF₆⁻) and bis(trifluoromethanesulfonyl)imide (TFSI⁻) anions (Scheme 1). All products were characterized with NMR and mass spectrometry, and we concluded that the products have enough purity for further optical and thermal analyses.



Scheme 1. Syntheses of ionic salts.

Fortunately, it should be emphasized that BBK-PF₆ formed a good single green crystal for analysis with X-ray crystallography. It was clearly shown that the compound has the expected structure and axial chirality (Figure 1). Accordingly, each R_a (light blue) and S_a (pink) formed dimer pairs and the layered structure, proposing that both π-conjugated planes should have an interaction. The distance between the closest planes was 3.46 Å, which is reasonable for the formation of π–π interaction. The structural data suggest that the symmetric property of PF₆ anion and hydrogen bonds between fluoride and hydrogen could support crystallization.

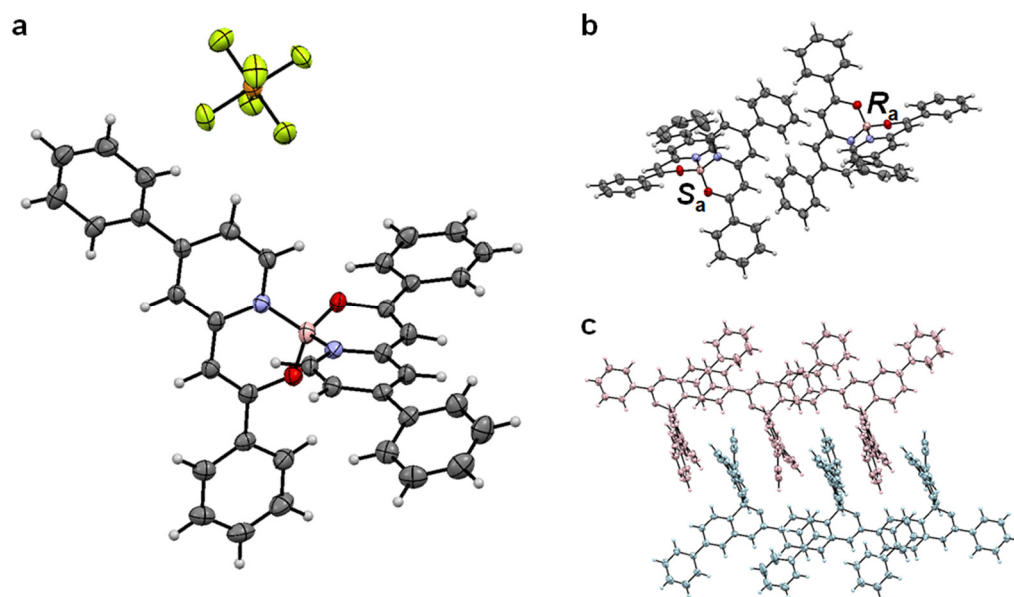


Figure 1. (a) ORTEP drawings of BBK-PF₆ (black—C; blue—N; red—O; white—H; light green—F; orange—P). (b) Axial chirality pair of the BBK unit; eliminated PF₆[−]. (c) Packing structure of chiral pair of the BBK unit; eliminated PF₆[−] (blue—R_a, pink—S_a).

Thermal properties, such as decomposition temperatures (T_{ds}) and melting temperatures (T_{ms}), were measured with thermogravimetric analysis (TGA) and differential scanning calorimetry (DSC), respectively (Table 1 and Figures S1 and S2). The T_d value of BBK-TFSI was higher than that of others. It is suggested that thermal motions should be suppressed in BBK-TFSI because the molecular weight of TFSI[−] is the largest of the four anions. In addition, we estimated their weight losses from the TGA profiles and observed that each decrease was equal to molecular weight of anion species, meaning that initial degradation occurs at the anion moieties. In the DSC results, it was clearly shown that all compounds have T_m below 100 °C, indicating that all ionic salts can be classified as an ionic liquid [46–48]. Two ligands with the spiro structures could play a

critical role in lowering T_m s by disturbing intermolecular interaction in the crystalline state. Moreover, symmetric structures of cations might contribute to lowering T_m s, as observed in the nano-cluster-containing ionic liquids [49,50].

Table 1. Optical properties of the ionic salts with variable anion.

	BBK-Cl	BBK-PF ₆	BBK-OTf	BBK-TFSI	M ^f
$\lambda_{\text{abs,sol}}$ [nm] ^a	391	391	393	394	380
ϵ [M ⁻¹ cm ⁻¹] ^a	39,200	19,000	33,300	34,800	22,300
$\lambda_{\text{em,solution}}$ [nm] ^a	453	453	455	453	460
Φ_{solution} ^{a,b}	0.26	0.24	0.26	0.26	0.35
τ [ns] ^c	1.3	1.4	1.4	1.4	0.5
	($\chi^2 = 1.12$)	($\chi^2 = 1.15$)	($\chi^2 = 1.03$)	($\chi^2 = 1.15$)	($\chi^2 = 1.01$)
k_f [$\times 10^8$ s ⁻¹]	1.8	1.7	1.8	1.8	3.7
k_{nr} [$\times 10^8$ s ⁻¹]	5.7	5.4	5.2	5.3	18.1
T_d (°C) ^d	214	218	193	233	
T_m (°C) ^e	75	65	68	55	

^a Measured in CH₂Cl₂ (1.0×10^{-5} mol/L). ^b Calculated as an absolute value determined using an integrated sphere method. ^c Fluorescence lifetime: excited at 375 nm, detected at $\lambda_{\text{em,sol}}$. ^d Determined from the onset in TGA profiles. ^e Determined from DSC. ^f Reprinted with permission from ref. [20]. Copyright 2017 John Wiley and Sons.

To investigate electronic structures in the ground state, UV–vis absorption spectra in CH₂Cl₂ solution were measured. The peak wavelength of BBK-Cl was found at 392 nm (Figure 2a and Table 1). Compared with ketoiminate difluoride M as a model compound, the peak appeared in the longer-wavelength region. This result suggests that electronic interaction should be caused through the central boron atom. We also examined absorption properties through anion exchanges (Figure 2a and Table 1). Accordingly, significant changes were hardly observed, indicating anion species hardly affect the electronic structures of the ionic salts.

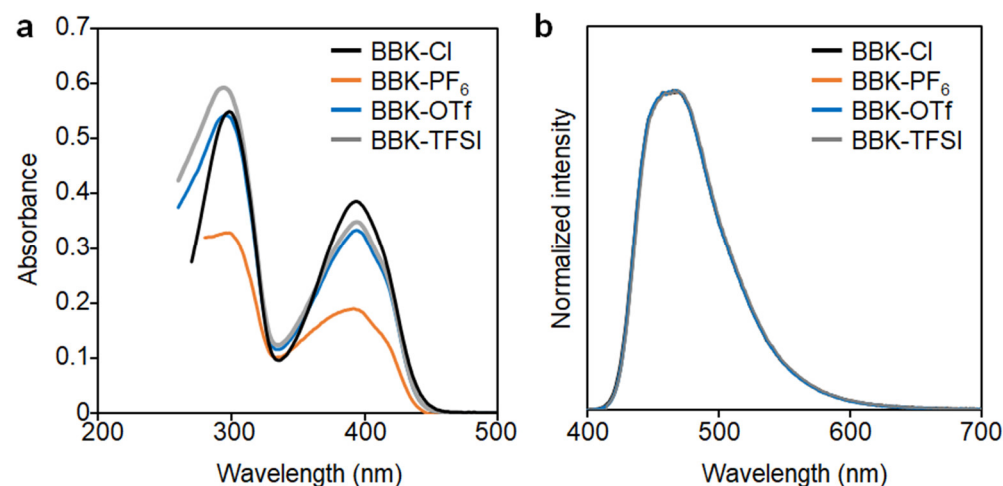


Figure 2. (a) UV–vis absorption and (b) emission spectra of the ionic salts in CH₂Cl₂ solution (1.0×10^{-5} mol/L). Emission spectra were obtained with the excitation light at $\lambda_{\text{abs,max}}$.

We measured emission spectra with three kinds of the ionic salts in dichloromethane (Figure 2b and Table 1). BBK-Cl showed the emission band in the blue region in the solution state, and slight differences were observed through anion exchange, indicating that anion hardly played a role in optical properties. Similar to the absorption properties, anion species hardly influence electronic structures of the ligand moieties in solution (Figure 2b and Table 1). Meanwhile, emission bands of the ionic salts were observed in the shorter wavelength region compared to that of M. According to the previous reports, the optical properties can be rationally explained [19,20]. The ligand potential shows a

larger degree of structural relaxation in the excited state. Through the formation of the spiro structures, structural relaxation could be disturbed, followed by emission bands in the shorter-wavelength region. The smaller rate constant of non-radiation decay of the ionic salts comparing to that of **M** strongly supports the suppression of molecular motions in the excited state by the spiro formation.

Since the crystalline sample was possible to obtain from BBK-PF₆, we monitored changes in luminescent properties in solid (Figures 3 and S4, Tables 1 and S2). It should be emphasized that BBK-PF₆ can exhibit emission in crystal ($\Phi_{\text{PL}} = 0.10$, Tables 1 and S1). The crystal sample of BBK-PF₆ exhibited green emission with the peak at 507 nm (Figure 3a). When the sample was scratched, the emission band shifted to the blue region by 30 nm and emission color was changed to light blue (Figure 3b,c). These data represent that BBK-PF₆ has a mechanochromic fluorescent property. This specific property should originate from changes in intermolecular interaction through π - π stacking during the morphology change from crystal to amorphous (Figure S3, Supplementary Materials) [51,52]. In the crystalline state, BBK-PF₆ formed ordered structures and had strong π - π intermolecular interaction between each chirality pair (Figure 1c). As a result, the emission band was observed in the longer-wavelength region. On the other hands, when that ordered packing was crumbled by mechanical stress, intermolecular interaction should decrease. Consequently, the emission band appeared in the shorter wavelength region. Their quantum yields before and after grinding were 0.10 and 0.15, respectively. These data support that loss of π - π intermolecular interaction should be responsible for emission in the condensed state. It should be mentioned that the mechanochromic luminescent property was obtained only from BBK-PF₆ which can form single crystals. Relatively higher crystallinity of the PF₆ salt should be favorable for exhibiting luminochromism through molecular environmental changes.

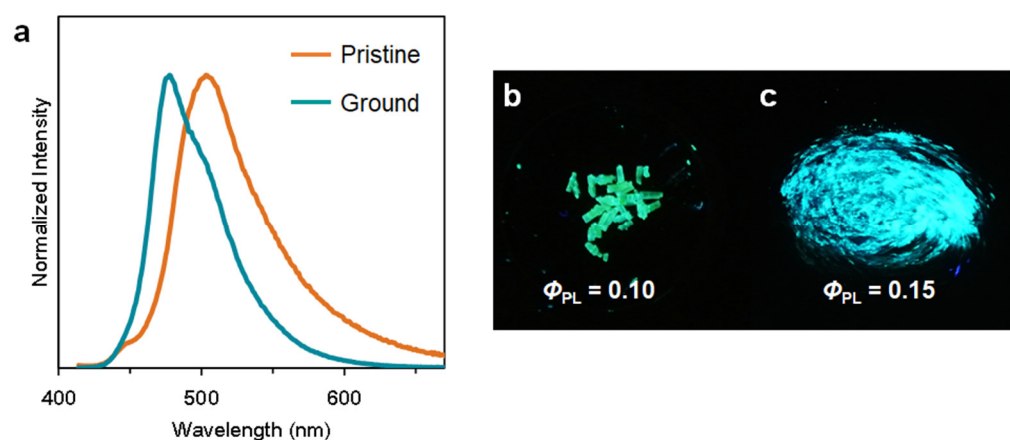


Figure 3. (a) Fluorescent spectra of BBK-PF₆ in the solid states (orange—crystalline pristine sample; blue—ground sample). Photographs of BBK-PF₆ under UV irradiation (b) before and (c) after grinding.

3. Experimental Section

General: ¹H (400 MHz), ¹¹B (128 MHz), and ¹³C (100 MHz) NMR spectra were recorded on a JEOL JNM-EX400 or a JEOL JNM-AL400 spectrometers (JEOL Ltd., Tokyo, Japan). In ¹H and ¹³C NMR spectra, tetramethylsilane (TMS) was used as an internal standard in CDCl₃, and ¹¹B NMR spectra were referenced externally to BF₃·OEt₂ (sealed capillary). UV–vis absorption spectra were recorded on a SHIMADZU UV-3600 spectrophotometer (Shimadzu Corporation, Kyoto, Japan). Photoluminescence (PL) spectra were measured with a HORIBA JOBIN YVON Fluorolog spectrofluorometer (HORIBA, Ltd., Kyoto, Japan), and photoluminescence quantum yields were calculated by the integrating sphere method. Fluorescence lifetime analyses were carried out on a Horiba FluoreCube spectrofluorometer system (HORIBA, Ltd., Kyoto, Japan); excitation at 375 nm using a UV diode laser (NanoLED-375L). Elemental analysis was performed at the Microanalytical Center of Ky-

oto University. DSC thermograms were carried out on a SII DSC 6220 instrument (Seiko Instruments Inc., Chiba, Japan). The sample on the aluminum pan was heated at the rate of 10 °C/min under nitrogen flowing (50 mL/min). Thermogravimetric analysis (TGA) was recorded on a Seiko Instruments Inc. (Chiba, Japan) EXSTAR TG/DTA6000. X-ray crystallographic analyses were carried out by Rigaku R-AXIS RAPID-F graphite-monochromated Mo K α radiation diffractometer with an imaging plate. A symmetry-related absorption correction was carried out using the program ABSCOR [53]. The analysis was carried out with direct methods (SHELX-97 [54] or SIR92 [55]) using Yadokari-XG [56]. The program ORTEP35 was used to generate the X-ray structural diagram [57,58]. Powder X-ray diffraction (PXRD) patterns were taken by using CuK α radiation with Rigaku Miniflex (Rigaku Corporation, Tokyo, Japan).

Synthesis of **M**: BF₃·Et₂O (6.2 mL, 7.11 g, 50.1 mmol) was added to the solution of **1** [20] (1.37 g, 5.0 mmol) in the mixed solvent of CH₂Cl₂ (30 mL) and NEt₃ (6 mL). The reaction mixture was refluxed under Ar atmosphere for 24 h and then cooled at r.t. The organic layer was washed with water (100 mL × 2) and brine (100 mL), dried over anhydrous magnesium sulfate, and concentrated by a rotary evaporator. The resulting solid was purified by silica gel column chromatography eluted with hexane/AcOEt (2/1). The product **M** was obtained after it was recrystallized from ethanol as an orange crystal (0.81 g, 50%). ¹H NMR (CDCl₃): δ 8.47 (1H, d, J = 6.2 Hz, Ar-H), 7.97 (2H, dd, J = 6.8, 1.7 Hz), 7.70 (2H, dd, J = 5.9, 2.1 Hz), 7.56 (1H, s), 7.55 (2H, d, J = 2.6 Hz), 7.49 (2H, d, J = 5.3 Hz), 7.45 (3H, m), 6.44 (1H, s) ppm. ¹³C NMR (CDCl₃): δ 163.1, 153.7, 151.9, 140.2, 136.1, 134.3, 130.9, 130.8, 129.5, 128.5, 127.3, 126.6, 119.5, 118.5, 93.4 ppm. ¹¹B NMR (CDCl₃): δ 1.47 ppm. HRMS (ESI): Calculated for [M + H]⁺, 322.1209; found, m/z 322.1209.

Synthesis of **BBK-Cl**: BCl₃ in CH₂Cl₂ solution (1.6 mL, 187 mg, 1.60 mmol) was added to the solution of **1** (918 mg, 3.36 mmol) in the mixed solvent of CH₂Cl₂ (24 mL) and NEt₃ (6.4 mL). The reaction mixture was stirred at r.t. under Ar atmosphere for 12 h. After removing solvents using a rotary evaporator, the yellow residue was dissolved into DMSO and precipitated into a large amount of Et₂O. The precipitation was recrystallized from Et₂O and MeOH. The product **BBK-Cl** was obtained as a yellow solid (326 mg, 36%). ¹H NMR (DMSO-*d*₆): δ 8.44 (1H, d, J = 6.6 Hz, Ar-H), 8.34 (1H, d, J = 2.0 Hz, Ar-H), 8.01 (2H, dd, J = 5.1, 1.7 Hz, Ar-H), 7.94–7.90 (3H, m, Ar-H), 7.70–7.50 (6H, m, Ar-H), 7.33 (1H, s, Ar-H) ppm. ¹³C NMR (DMSO-*d*₆): δ 153.7, 151.0, 141.8, 134.6, 132.8, 131.5, 131.4, 129.6, 129.0, 127.6, 127.1, 126.0, 120.8, 120.3, 95.0 ppm. ¹¹B NMR (DMSO-*d*₆): δ 4.12 ppm. HRMS (ESI): Calculated for [M + H]⁺, 555.2238; found, m/z 555.2235.

Synthesis of **BBK-PF₆**: **BBK-Cl** (200 mg, 0.34 mmol) was dissolved into MeOH (5 mL) and added to the solution of silver hexafluorophosphate (105 mg, 0.37 mmol) in acetonitrile (5 mL). After stirring at r. t. for 2 h, the solution was filtered to remove white precipitate. The obtained precipitate was extracted with CH₂Cl₂ and washed with water twice. The resulting yellow solution was concentrated using a rotary evaporator and redissolved into benzene. After freeze-drying, **BBK-PF₆** was obtained as a yellow solid (80%, 190 mg). ¹H NMR (CDCl₃): δ 8.08 (1H, d, J = 6.6 Hz, Ar-H), 7.92 (2H, dd, J = 7.8, 1.2 Hz, Ar-H), 7.80–7.76 (3H, m, Ar-H), 7.94–7.90 (1H, dd, J = 6.6, 2.0 Hz, Ar-H), 7.60–7.44 (6H, m, Ar-H), 6.81 (1H, s, Ar-H) ppm. ¹³C NMR (DMSO-*d*₆): δ 153.8, 151.0, 141.8, 134.6, 132.8, 131.5, 131.4, 129.6, 129.0, 127.6, 127.1, 126.0, 120.8, 120.3, 95.1 ppm. ¹¹B NMR (DMSO-*d*₆): δ 4.12 ppm. HRMS (ESI): Calculated for [M + H]⁺, 555.2238; found, m/z 555.2235. Calculated for [PF₆][−], 144.9647; found, m/z 144.9644. CCDC #: 2071316.

Synthesis of **BBK-OTf**: **BBK-OTf** was prepared from **BBK-Cl** (200 mg, 0.34 mmol) and silver trifluoromethanesulfonate (96 mg, 0.37 mmol) as yellow solid according to the same method with **BBK-PF₆**. ¹H NMR (DMSO-*d*₆): δ 8.44 (1H, d, J = 6.6 Hz, Ar-H), 8.32 (1H, s, Ar-H), 8.01 (2H, dd, J = 5.1, 1.7 Hz, Ar-H), 7.94–7.90 (3H, m, Ar-H), 7.70–7.50 (6H, m, Ar-H), 7.31 (1H, s, Ar-H) ppm. ¹³C NMR (DMSO-*d*₆): δ 153.7, 151.0, 144.0, 141.8, 134.6, 132.8, 131.5, 131.4, 129.6, 129.0, 127.7, 127.2, 126.0, 120.8, 120.3, 95.1 ppm. ¹¹B NMR (DMSO-*d*₆): δ 4.12 ppm. HRMS (ESI): Calculated for [M + H]⁺, 555.2238; found, m/z 555.2235. HRMS

(ESI): Calculated for $[M + H]^+$, 555.2238; found, m/z 555.2236. Calculated for $[OTf]^-$, 148.9526; found, m/z 148.9522.

Synthesis of BBK-TFSI: BBK-TFSI was prepared from BBK-Cl (200 mg, 0.34 mmol) and silver bis(trifluoromethanesulfonyl)imide (144 mg, 0.37 mmol) as yellow solid according to the same method with BBK-PF₆. ¹H NMR (DMSO-*d*₆): δ 8.44 (1H, d, *J* = 6.6 Hz, Ar-H), 8.32 (1H, d, *J* = 2.0 Hz, Ar-H), 8.01 (2H, dd, *J* = 7.3, 3.6 Hz, Ar-H), 7.94–7.90 (3H, m, Ar-H), 7.70–7.50 (6H, m, Ar-H), 7.31 (1H, s, Ar-H) ppm. ¹³C NMR (DMSO-*d*₆): δ 158.6, 153.8, 141.8, 140.2, 134.6, 132.8, 131.5, 131.4, 129.6, 129.0, 127.6, 127.1, 126.0, 120.8, 120.3, 95.1 ppm. ¹¹B NMR (DMSO-*d*₆): δ 4.12 ppm. HRMS (ESI): Calculated for $[M + H]^+$, 555.2238; found, m/z 555.2235. HRMS (ESI): Calculated for $[M + H]^+$, 555.2238; found, m/z 555.2236. Calculated for $[TFSI]^-$, 279.9178; found, m/z 279.9175.

4. Conclusions

By employing the luminescent boron complex structure, we obtained luminescent ionic salts with various kinds of anions. Since the *T*_m values were found below 100 °C, these salts can be classified as an ionic liquid. All molecules show intense emission not only in solution but also in solid. By replacing the counter anion, the crystallinity can be altered. In particular, it was found that the PF₆ salt can form a single crystal and an X-ray analysis was applicable. Furthermore, we accomplished detection of luminochromism from crystal to amorphous state using mechanical stimuli. It is proposed that our stimuli-responsive luminescent materials might be potentially applicable to introduce environment-monitoring ability in the conventional usages of ionic liquids, such as electrolytes in lithium batteries and thermal-resistant reaction solvents.

Supplementary Materials: The following supporting information can be downloaded at: <https://www.mdpi.com/article/10.3390/molecules27113438/s1>, Figure S1: TGA diagrams of BBK salts under N₂ flowing; Figure S2: DSC profiles of BBK salts; Figure S3: XRD profiles of BBK-PF₆ before and after the mechanical treatment; Figure S4: Solid-state luminescent properties of BBK salts; Figure S5: ¹H NMR spectrum of BBK-Cl in DMSO-*d*₆; Figure S6: ¹³C NMR spectrum of BBK-Cl in DMSO-*d*₆; Figure S7: ¹¹B NMR spectrum of BBK-Cl in DMSO-*d*₆; Figure S8: ¹H NMR spectrum of BBK-PF₆ in CDCl₃; Figure S9: ¹³C NMR spectrum of BBK-PF₆ in DMSO-*d*₆; Figure S10: ¹¹B NMR spectrum of BBK-PF₆ in DMSO-*d*₆; Figure S11: ¹H NMR spectrum of BBK-OTf in DMSO-*d*₆; Figure S12: ¹³C NMR spectrum of BBK-OTf in DMSO-*d*₆; Figure S13: ¹¹B NMR spectrum of BBK-OTf in DMSO-*d*₆; Figure S14: ¹H NMR spectrum of BBK-TFSI in DMSO-*d*₆; Figure S15: ¹³C NMR spectrum of BBK-TFSI in DMSO-*d*₆; Figure S16: ¹¹B NMR spectrum of BBK-TFSI in DMSO-*d*₆; Table S1: Optical properties of BBK-PF₆; Table S2: Solid-state luminescent properties of BBK salts.

Author Contributions: Conceptualization, K.S. and K.T.; methodology, K.S.; validation, K.S. and S.I.; formal analysis, K.S. and S.I.; investigation, K.S. and S.I.; writing—original draft preparation, K.S., S.I. and K.T.; writing—review and editing, K.T. and Y.C.; supervision, K.T. and Y.C.; funding acquisition, K.T. and Y.C. All authors have read and agreed to the published version of the manuscript.

Funding: This work was partially funded by the Toyo Gosei Memorial Foundation and JSPS KAK-ENHI Grant Numbers JP21H02001 and JP21K19002 (for K.T.).

Institutional Review Board Statement: Not applicable.

Informed Consent Statement: Not applicable.

Data Availability Statement: The data presented in this study are available in article and Supplementary Materials.

Conflicts of Interest: The authors declare no conflict of interest.

Sample Availability: Samples of the compounds are not available from the authors.

References

1. Li, J.; Wang, J.; Li, H.; Song, N.; Wang, D.; Tang, B.Z. Supramolecular materials based on AIE luminogens (AIEgens): Construction and applications. *Chem. Soc. Rev.* **2020**, *49*, 1144–1172. [[CrossRef](#)]
2. Chua, M.H.; Zhou, H.; Zhu, Q.; Tang, B.Z.; Xu, J.W. Recent advances in cation sensing using aggregation-induced emission. *Mater. Chem. Front.* **2021**, *5*, 659–708. [[CrossRef](#)]
3. Han, T.; Wang, X.; Wang, D.; Tang, B.Z. Functional Polymer Systems with Aggregation-Induced Emission and Stimuli Responses. *Top. Curr. Chem.* **2021**, *379*, 7. [[CrossRef](#)]
4. Mise, Y.; Imoto, K.; Ogi, T.; Tsunoji, N.; Ooyama, Y. Fluorescence sensors for detection of water based on tetraphenylethene–anthracene possessing both solvatofluorochromic properties and aggregation-induced emission (AIE) characteristics. *New J. Chem.* **2021**, *45*, 4164–4173. [[CrossRef](#)]
5. Ooyama, Y.; Sagisaka, R.; Enoki, T.; Tsunoji, N.; Ohshita, J. Tetraphenylethene– and Diphenyldibenzofulvene–anthracene-based Fluorescence Sensors Possessing Photo-induced Electron Transfer and Aggregation-induced Emission Enhancement Characteristics for Detection of Water. *New J. Chem.* **2018**, *42*, 13339–13350. [[CrossRef](#)]
6. Jiang, B.; Zhang, C.W.; Shi, X.L.; Yang, H.B. AIE-active Metal-organic Coordination Complexes Based on Tetraphenylethylene Unit and Their Applications. *Chin. J. Polym. Sci.* **2019**, *37*, 372–382. [[CrossRef](#)]
7. Alam, P.; Climent, C.; Alemany, P.; Laskar, I.R. “Aggregation-induced emission” of transition metal compounds: Design, mechanistic insights, and applications. *J. Photochem. Photobiol. C Photochem. Rev.* **2019**, *41*, 100317. [[CrossRef](#)]
8. Li, D.; Yu, J. AIEgens-Functionalized Inorganic-Organic Hybrid Materials: Fabrications and Applications. *Small* **2016**, *12*, 6478–6494. [[CrossRef](#)] [[PubMed](#)]
9. Sathish, V.; Ramdass, A.; Thanasekaran, P.; Lu, K.L.; Rajagopal, S. Aggregation-induced phosphorescence enhancement (AIPE) based on transition metal complexes—An overview. *J. Photochem. Photobiol. C Photochem. Rev.* **2015**, *23*, 25–44. [[CrossRef](#)]
10. Chujo, Y.; Tanaka, K. New Polymeric Materials Based on Element-Blocks. *Bull. Chem. Soc. Jpn.* **2015**, *88*, 633–643. [[CrossRef](#)]
11. Gon, M.; Tanaka, K.; Chujo, Y. Recent Progress in the Development of Advanced Element-Block Materials. *Polym. J.* **2018**, *50*, 109–126. [[CrossRef](#)]
12. Gon, M.; Tanaka, K.; Chujo, Y. Concept of Excitation-Driven Boron Complexes and Their Applications for Functional Luminescent Materials. *Bull. Chem. Soc. Jpn.* **2019**, *92*, 7–18. [[CrossRef](#)]
13. Ito, S.; Gon, M.; Tanaka, K.; Chujo, Y. Molecular Design and Applications of Luminescent Materials Composed of Group 13 Elements with an Aggregation-Induced Emission Property. *Natl. Sci. Rev.* **2021**, *8*, nwab049. [[CrossRef](#)] [[PubMed](#)]
14. Ito, S.; Gon, M.; Tanaka, K.; Chujo, Y. Recent Developments in Stimuli-Responsive Luminescent Polymers Composed of Boron Compounds. *Polym. Chem.* **2021**, *12*, 6372–6380. [[CrossRef](#)]
15. Gon, M.; Ito, S.; Tanaka, K.; Chujo, Y. Design Strategies and Recent Results for Near-Infrared-Emissive Materials Based on Element-Block π -Conjugated Polymers. *Bull. Chem. Soc. Jpn.* **2021**, *94*, 2290–2301. [[CrossRef](#)]
16. Tanaka, K.; Chujo, Y. Modulation of the Solid-state Luminescent Properties of Conjugated Polymers by Changing the Connecting Points of Flexible Boron Element-Blocks. *Polym. J.* **2020**, *52*, 555–566. [[CrossRef](#)]
17. Tanaka, K.; Chujo, Y. Recent Progress of Optical Functional Nanomaterials Based on Organoboron Complexes with β -Diketonate, Ketoiminate and Diiminate. *NPG Asia Mater.* **2015**, *7*, e223. [[CrossRef](#)]
18. Yamaguchi, M.; Ito, S.; Hirose, A.; Tanaka, K.; Chujo, Y. Luminescent Color Tuning with Polymer Films Composed of Boron Diiminate Conjugated Copolymers by Changing Connection Points to Comonomers. *Polym. Chem.* **2018**, *9*, 1942–1946. [[CrossRef](#)]
19. Yamaguchi, M.; Ito, S.; Hirose, A.; Tanaka, K.; Chujo, Y. Control of Aggregation-Induced Emission versus Fluorescence Aggregation-Caused Quenching by the Bond Existence at the Single Site in Boron Pyridinoiminate Complexes. *Mater. Chem. Front.* **2017**, *1*, 1573–1579. [[CrossRef](#)]
20. Suenaga, K.; Tanaka, K.; Chujo, Y. Design and Luminescent Chromism of Fused Boron Complexes Having Constant Emission Efficiencies in Solution, Amorphous and Crystalline States. *Eur. J. Org. Chem.* **2017**, *2017*, 5191–5196. [[CrossRef](#)]
21. Yamaguchi, M.; Tanaka, K.; Chujo, Y. Control of Solution and Solid-State Emission with Conjugated Polymers Based on the Boron Pyridinoiminate Structure by Ring Fusion. *Polymer* **2018**, *142*, 127–131. [[CrossRef](#)]
22. Kawano, Y.; Ito, Y.; Ito, S.; Tanaka, K.; Chujo, Y. π -Conjugated Copolymers Composed of Boron Formazanate and Their Application for a Wavelength Converter to Near-Infrared Light. *Macromolecules* **2021**, *54*, 1934–1942. [[CrossRef](#)]
23. Ito, S.; Fukuyama, M.; Tanaka, K.; Chujo, Y. Effects of Regioregularity of π -Conjugated Polymers Composed of Boron β -Diketiminato on Their Stimuli-Responsive Luminescence. *Macromol. Chem. Phys.* **2022**, *223*, 2100504. [[CrossRef](#)]
24. Ito, S.; Yaegashi, M.; Tanaka, K.; Chujo, Y. Reversible Vapochromic Luminescence Accompanied by Planar Half-Chair Conformational Change of a Propeller-Shaped Boron β -Diketiminato Complex. *Chem. Eur. J.* **2021**, *27*, 9302–9312. [[CrossRef](#)] [[PubMed](#)]
25. Suenaga, K.; Tanaka, K.; Chujo, Y. The Positive Luminescent Sensor for Aerobic Conditions Based on Polyhedral Oligomeric Silsesquioxane Networks. *Chem. Res. Chin. Univ.* **2021**, *37*, 162–165. [[CrossRef](#)]
26. Suenaga, K.; Tanaka, K.; Chujo, Y. Heat-Resistant Mechanoluminescent Chromism of the Hybrid Molecule Based on Boron Ketoiminate Modified Octa-Substituted Polyhedral Oligomeric Silsesquioxane. *Chem. Eur. J.* **2017**, *23*, 1409–1414. [[CrossRef](#)] [[PubMed](#)]

27. Suenaga, K.; Yoshii, R.; Tanaka, K.; Chujo, Y. Sponge-Type Emissive Chemosensors for the Protein Detection Based on Boron Ketoiminate-Modifying Hydrogels with Aggregation-Induced Blue Shift Emission Property. *Macromol. Chem. Phys.* **2016**, *217*, 414–417. [[CrossRef](#)]
28. Saotome, S.; Suenaga, K.; Tanaka, K.; Chujo, Y. Design for Multi-step Mechanochromic Luminescence Property by Enhancement of Environmental Sensitivity in a Solid-state Emissive Boron Complex. *Mater. Chem. Front.* **2020**, *4*, 1781–1788. [[CrossRef](#)]
29. Suenaga, K.; Uemura, K.; Tanaka, K.; Chujo, Y. Stimuli-Responsive Luminochromic Polymers Consisting of Multi-States Emissive Fused Boron Ketoiminate. *Polym. Chem.* **2020**, *11*, 1127–1133. [[CrossRef](#)]
30. Ito, S.; Tanaka, K.; Chujo, Y. Characterization and Photophysical Properties of a Luminescent Aluminum Hydride Complex Supported by a β -Diketiminato Ligand. *Inorganics* **2019**, *7*, 100. [[CrossRef](#)]
31. Ito, S.; Hirose, A.; Yamaguchi, M.; Tanaka, K.; Chujo, Y. Size-Discrimination for Volatile Organic Compounds Utilizing Gallium Diiminate by Luminescent Chromism of Crystallization-Induced Emission via Encapsulation-Triggered Crystal-Crystal Transition. *J. Mater. Chem. C* **2016**, *3*, 5564–5571. [[CrossRef](#)]
32. Ito, S.; Hirose, A.; Yamaguchi, M.; Tanaka, K.; Chujo, Y. Synthesis of Aggregation-Induced Emission-Active Conjugated Polymers Composed of Group 13 Diiminate Complexes with Tunable Energy Levels via Alteration of Central Element. *Polymers* **2017**, *9*, 68–78. [[CrossRef](#)] [[PubMed](#)]
33. Yamaguchi, M.; Tanaka, K.; Chujo, Y. Design of Conjugated Molecules Presenting Short-Wavelength Luminescence by Utilizing Heavier Atoms of the Same Element Group. *Chem. Asian J.* **2018**, *13*, 1342–1347. [[CrossRef](#)] [[PubMed](#)]
34. Chen, X.; Zhang, X.; Zhang, G. Wide-range thermochromic luminescence of organoboronium complexes. *Chem. Commun.* **2015**, *51*, 161–163. [[CrossRef](#)] [[PubMed](#)]
35. Zhang, X.; Zhang, G. Hydrochromic fluorescence of organo-boronium-avobenzene complexes. *Anal. Methods* **2012**, *4*, 2641–2643. [[CrossRef](#)]
36. Sakamoto, R.; Iwashima, T.; Kögel, J.F.; Kusaka, S.; Tsuchiya, M.; Kitagawa, Y.; Nishihara, H. Dissymmetric Bis(dipyrinato)zinc(II) Complexes: Rich Variety and Bright Red to Near-Infrared Luminescence with a Large Pseudo-Stokes Shift. *J. Am. Chem. Soc.* **2016**, *138*, 5666–5677. [[CrossRef](#)]
37. Braunschweig, H.; Krummenacher, I.; Mailänder, L.; Pentecost, L.; Vargas, A. Formation of a stable radical by oxidation of a tetraorganoborate. *Chem. Commun.* **2016**, *52*, 7005–7008. [[CrossRef](#)]
38. Durka, K.; Głowacki, I.; Luliński, S.; Łuszczynska, B.; Smętek, J.; Szczepanik, P.; Serwatowski, J.; Wawrzyniak, U.E.; Wesela-Bauman, G.; Witkowska, E.; et al. Efficient 8-oxyquinolino emitters based on a 9,10-dihydro-9,10-diboraanthracene scaffold for applications in optoelectronic devices. *J. Mater. Chem. C* **2015**, *3*, 1354–1364. [[CrossRef](#)]
39. Fumanal, M.; Mota, F.; Novoa, J.J.; Ribas-Arino, J. Unravelling the Key Driving Forces of the Spin Transition in π -Dimers of Spiro-biphenalenyl-Based Radicals. *J. Am. Chem. Soc.* **2015**, *137*, 12843–12855. [[CrossRef](#)]
40. Sarkar, A.; Pal, S.K.; Itkis, M.E.; Tham, F.S.; Haddon, R.C. Sulfur and selenium substituted spiro-biphenalenyl-boron neutral radicals. *J. Mater. Chem.* **2012**, *22*, 8245–8256. [[CrossRef](#)]
41. Bag, P.; Pal, S.K.; Itkis, M.E.; Sarkar, A.; Tham, F.S.; Donnadieu, B.; Haddon, R.C. Synthesis of Tetrachalcogenide-Substituted Phenalenyl Derivatives: Preparation and Solid-State Characterization of Bis(3,4,6,7-tetrathioalkyl-phenalenyl)boron Radicals. *J. Am. Chem. Soc.* **2013**, *135*, 12936–12939. [[CrossRef](#)] [[PubMed](#)]
42. Bag, P.; Itkis, M.E.; Stekovic, D.; Pal, S.K.; Tham, F.S.; Haddon, R.C. Switching Closed-Shell to Open-Shell Phenalenyl: Toward Designing Electroactive Materials. *J. Am. Chem. Soc.* **2015**, *137*, 10000–10008. [[CrossRef](#)] [[PubMed](#)]
43. Ohkuma, H.; Nakagawa, T.; Shizu, K.; Yasuda, T.; Adachi, C. Thermally activated delayed fluorescence from a spiro-diazafluorene derivative. *Chem. Lett.* **2014**, *43*, 1017–1019. [[CrossRef](#)]
44. Saragi, T.P.I.; Pudzich, R.; Fuhrmann, T.; Salbeck, J. Organic phototransistor based on intramolecular charge transfer in a bifunctional spiro compound. *Appl. Phys. Lett.* **2004**, *84*, 2334–2336. [[CrossRef](#)]
45. Schneider, D.; Rabe, T.; Tiedl, T.; Dobbertin, T.; Kroeger, M.; Becker, E.; Johannes, H.H.; Kowalsky, W.; Weimann, T.; Wang, J.; et al. Broadband tuning of external cavity bound-to-continuum quantum-cascade lasers. *Appl. Phys. Lett.* **2004**, *84*, 1659–1661. [[CrossRef](#)]
46. Tanaka, K.; Ishiguro, F.; Jeon, J.-H.; Hiraoka, T.; Chujo, Y. POSS Ionic Liquid Crystals. *NPG Asia Mater.* **2015**, *7*, e174. [[CrossRef](#)]
47. Tanaka, K.; Hiraoka, T.; Ishiguro, F.; Jeon, J.-H.; Chujo, Y. Adamantane Ionic Liquids. *RSC Adv.* **2014**, *4*, 28107–28110. [[CrossRef](#)]
48. Tanaka, K.; Ishiguro, F.; Chujo, Y. POSS Ionic Liquid. *J. Am. Chem. Soc.* **2010**, *132*, 17649–17651. [[CrossRef](#)]
49. Hasebe, R.; Kaneko, Y. Control of crystalline-amorphous structures of polyhedral oligomeric silsesquioxanes containing two types of ammonium side-chain groups and their properties as protic ionic liquids. *Molecules* **2019**, *24*, 4553. [[CrossRef](#)]
50. Maeda, D.; Ishii, T.; Kaneko, Y. Effect of lengths of substituents in imidazolium groups on the preparation of imidazolium-salt-type ionic liquids containing polyhedral oligomeric silsesquioxane structures. *Bull. Chem. Soc. Jpn.* **2018**, *91*, 1112–1119. [[CrossRef](#)]
51. Imoto, H.; Kizaki, K.; Watase, S.; Matsukawa, K.; Naka, K. Color Tuning of the Aggregation-Induced Emission of Maleimide Dyes by Molecular Design and Morphology Control. *Chem. Eur. J.* **2015**, *21*, 12105–12111. [[CrossRef](#)] [[PubMed](#)]
52. Imoto, H.; Nohmi, K.; Kizaki, K.; Watase, S.; Matsukawa, K.; Yamamoto, S.; Mitsuishi, M.; Naka, K. Effect of alkyl groups on emission properties of aggregation induced emission active N-alkyl arylaminomaleimide dyes. *RSC Adv.* **2015**, *5*, 94344–94350. [[CrossRef](#)]
53. Higashi, T. *ABSCOR. Program for Absorption Correction*; Rigaku Corporation: Tokyo, Japan, 1995.
54. Sheldrick, G.M. SHELXT—Integrated space-group and crystal-structure determination. *Acta Cryst. A* **2015**, *71*, 3–8. [[CrossRef](#)]

55. Sheldrick, G.M. Crystal structure refinement with SHELXL. *Acta Cryst. C* **2015**, *71*, 3–8. [[CrossRef](#)]
56. Wakita, K. Yadokari-XG, Program for Crystal Structure Analysis. 2001. Available online: <http://chem.s.kanazawa-u.ac.jp/coord/yadokari/y-citation.html> (accessed on 1 May 2022).
57. Hübschle, C.B.; Sheldrick, G.M.; Dittrich, B. ShelXle: A Qt graphical user interface for SHELXL. *J. Appl. Cryst.* **2011**, *44*, 1281–1284. [[CrossRef](#)] [[PubMed](#)]
58. Farrugia, L.J. ORTEP-3 for Windows—A version of ORTEP-III with a graphical user interface (GUI). *J. Appl. Cryst.* **1997**, *30*, 565. [[CrossRef](#)]